Journal of Alloys and Compounds 509 (2011) 4972–4977

Contents lists available at ScienceDirect

Journal of Alloys and Compounds

journal homepage: www.elsevier.com/locate/jallcom

Growth and photocatalytic activity of ZnO nanosheets stabilized by Ag nanoparticles

Danhui Zhang, Xiaoheng Liu*, Xin Wang*

Key Laboratory of Education Ministry for Soft Chemistry and Functional Materials, Nanjing University of Science and Technology, Nanjing 210094, China

ARTICLE INFO

Article history:
Received 1 December 2010
Received in revised form 9 January 2011
Accepted 21 January 2011
Available online 2 February 2011

Keywords:
ZnO sheets
Ag nanoparticles
(n-Dodecyl)trimethylammonium bromide
Two-phase method

ABSTRACT

The Ag nanoparticles-stabilized ZnO nanosheets were prepared using a liquid–liquid two-phase method with (n-Dodecyl)trimethylammonium bromide (DTAB) as a phase transfer agent at the room temperature. The silver nanoparticles which are conductors with the character of attracting energy can make the ZnO sheets stabilize under the higher energy electrons. The samples are characterized by X-ray diffraction (XRD), scanning electron microscopy (SEM), transmission electron microscopy (TEM), UV–vis spectroscopy and fluorescence. The results demonstrate that the silver nanoparticles load on the surface of ZnO sheets and make the ZnO sheets stabilize. Furthermore, the formation mechanism of ZnO sheets stabilized by silver nanoparticles was also proposed and discussed in detail. Moreover, the photocatalysis test shows that the ZnO sheets stabilized by silver nanoparticles exhibit a higher photocatalytic activity than the pure ZnO nanosheets, thereby implying that the Ag/ZnO interfaces promote the separation of photogenerated electron–hole pairs and enhance the photocatalytic activity.

1. Introduction

Zinc oxide (ZnO), as an n-type semiconductor with a wide band gap (3.37 eV) and a large exciton binding energy of 60 meV at room temperature [1] has received extensive scientific attention due to their photoluminescence (PL), field emission, and piezoelectric properties. Furthermore, ZnO nanocrystals have shown considerable potential as materials for ceramics, piezoelectric transducers, optical coatings, high speed and display devices, gas sensors, varistors, photo-catalysts, and photovoltaics [2,3]. Also the high chemical stability and low toxicity together make ZnO suitable for UV screening applications. For these reasons, many methods for the synthesis of ZnO nanoparticles have been developed, including microwave method [4], sol–gel process [5], solvo/hydrothermal reactions [6], precipitation [7], solution combustion method [8], spray pyrolysis [9], gas-phase condensation [10], thermal evaporation [11], direct milling [12], and mechanochemical reactions [13].

As we know, semiconductor metal oxides (SMOs) applied in the production of photoelectrochemical cells, gas sensors, field-effect transistor, surface acoustic wave devices, and photoluminescence devices have triggered much research activity [14]. For example, ZnO has significant advantages in optoelectronic applications such as ultraviolet lasing media owing to its extreme large binding energy of the exciton, can form the stable exciton [15]. However, the simplex SMO could not completely meet the increasing application needs in constructing high-performance semiconductor devices. Therefore, considerable efforts have been spent in enhancing physical and chemical properties of the SMOs, such as loading noble metals on the surface of SMOs, doping metals into the lattice of the SMOs, incorporating among the SMOs, and so on. Generally, one accepted solution is to modify the semiconductor metal oxides with noble metals, which could improve the photocatalytic, gas-sensing, and photoluminescence properties [16]. As a matter of fact, the interaction between the noble metals and the SMOs is complicated because the interaction relates to the carrier concentration, defect level, and surface states of the semiconductor, electronic, optical properties, and so forth. Therefore, good understanding of the interaction will facilitate the fundamental and technical application of the SMOs modified with noble metal.

In this work, we have successfully synthesized ZnO nanosheets stabilized by silver nanoparticles using a liquid–liquid two-phase method with (n-Dodecyl)trimethylammonium bromide (DTAB) as a phase transfer agent at the room temperature. Furthermore, the information of the samples was investigated using X-ray diffraction (XRD), scanning electron microscopy (SEM), transmission electron microscopy (TEM), UV–vis absorption spectroscopy (UV–vis), and photoluminescence (PL) spectroscopy, which was in an attempt to understand well the interaction between the silver and ZnO. Moreover, the formation mechanism of ZnO sheets stabilized by silver nanoparticles was also proposed and discussed in detail. The photocatalysis activities of ZnO sheets stabilized by silver nanoparticles and pure ZnO nanosheets were also displayed.

* Corresponding authors. Tel.: +86 25 84315943; fax: +86 25 84432747.
E-mail addresses: xhliu@mail.njust.edu.cn (X. Liu), wxin@public1.ptt.js.cn (X. Wang).

0925-8388/$ – see front matter © 2011 Elsevier B.V. All rights reserved.
doi:10.1016/j.jallcom.2011.01.145

2. Experimental

2.1. Materials

Zinc acetate dihydrate ($Zn(CHCOO)_2{\cdot}2H_2O$) was obtained from Shanghai Chem. Co. Silver nitrate ($AgNO_3$) and sodium borohydride ($NaBH_4$) were obtained from Aldrich. (n-Dodecyl)trimethylammonium bromide (DTAB) was obtained from A Johnson Matthey Co. 1-Dodecanethiol ($CH_3(CH_2)_{11}SH$) and other reagents were also supplied by Aldrich. All the reagents were used as received, without further purification, and all the water was deionized.

2.2. Syntheses of ZnO sheets

ZnO nanosheets were synthesized according to a modified version of a common two-phase system. A 30 mL aqueous solution of $Zn(CH_3COO)_2$ (0.05 M) was combined with 20 mL of a toluene solution of phase transfer agent (n-Dodecyl)trimethylammonium bromide (1.6 g DTAB) and vigorously stirred for 8 h. The organic phase, which contained the $Zn(OH)_2$ (Scheme 1), was isolated from the aqueous phase by phase separation. The product was washed in excess ethanol to remove the residual phase transfer agent in the organic phase. The final product was vacuum-dried at 60 °C for overnight.

2.3. Syntheses of ZnO sheets stabilized by silver nanoparticles

A 30 mL aqueous solution of $Zn(CH_3COO)_2$ (0.05 M) and $AgNO_3$ (0.03 M) were combined with 20 mL of a toluene solution of phase transfer agent (n-Dodecyl)trimethylammonium bromide (1.6 g DTAB) and vigorously stirred for 8 h. The organic phase, which contained the silver ions and $Zn(OH)_2$, was isolated from the aqueous phase by phase separation and 150 μL of 1-dodecanethiol was added. After the mixture was stirred for 15 min, the silver ions were reduced by introduction of 24 mL of an aqueous solution of $NaBH_4$ and then stirred for another 8 h. The organic phase was isolated from the aqueous phase by phase separation. The final product was washed in excess ethanol and acetone to remove the residual phase transfer agent and unbound thiol in the organic phase and then vacuum-dried at 60 °C for overnight. In this reaction system, not all the synthesized silver nanoparticles load on the ZnO sheets. According to the calculation (using the UV–vis spectra), 2.5% Ag nanoparticles are supported on the surface of ZnO.

2.4. Characterization

UV–vis spectra were recorded on a Shimadzu UV-1201 spectrophotometer in a 1 cm optical path quartz cuvette over a 200–800 nm range at room temperature. The X-ray diffraction (XRD) analyses were performed on a Bruker D8 Advance diffractometer with Cu Kα radiation. The diffraction data was recorded for 2θ angles between 10° and 80°. Morphology analyses of samples were carried out on JEOL-2100 transmission electron microscope (TEM). Scanning electron microscope (SEM) images were preformed on a JEOL JSM-6380LV SEM. Fluorescence spectrometer (RF-5301PC, Shimadzu) with a 150W Xenon lamp as the excitation light source at room temperature was used. For photocatalytic measurement, 10 mg of each catalyst was suspended in 200 mL of methyl orange aqueous solution (20 ppm), and then the mixture was put into quartz tubes and agitated about 3 h in the absence of light to attain equilibrium adsorption on the catalyst surface. Ultraviolet (UV) irradiation was carried out by using a 500 W fluorescent Hg-lamp. After a given irradiation time, about 3.5 mL of the mixture was withdrawn and the catalysts were separated through centrifugation. The photocatalytic degradation process was monitored by UV–vis spectrophotometer (UV-1201) to measure the absorption of methyl orange at the wavelength of 463 nm.

3. Results and discussion

3.1. The XRD patterns

Fig. 1 illustrates the XRD patterns of free Ag nanoparticles, pure ZnO sheets and ZnO sheets stabilized by Ag nanoparticles, where the XRD patterns of ZnO sheets and Ag nanoparticles products are also shown for comparison. The not perfect wurtzite ZnO and fcc Ag phases coexist in the Ag/ZnO crystals, and the XRD patterns match their JCPDS files Nos. 36-1451 and 04-0783, respectively [17,18]. Furthermore, no remarkable shifts of any diffraction peaks are detected, which indicates that the change in the lattice parameters of the ZnO nanocrystals is negligible. But the other peaks which are not marked may be assigned to the $ZnO{\cdot}nH_2O$.

The crystallographic structure of pure ZnO nanosheets dried at 130 °C higher temperature is characterized by XRD, as shown in Fig. 2. The obtained ZnO nanosheets are of wurtzite structure (hexagonal phase, space group P63mc), which can be well indexed

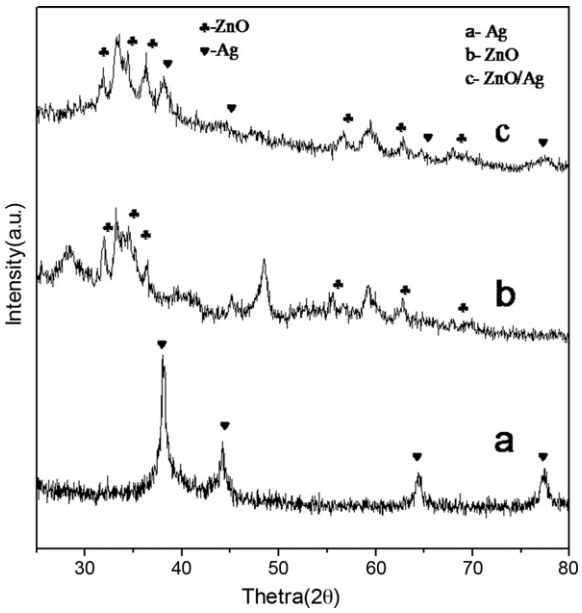

Fig. 1. XRD patterns of (a) Ag nanoparticles, (b) pure ZnO sheets and (c) ZnO sheets stabilized by Ag nanoparticles.

to the typical wurtzite structure of hexagonal ZnO phase reported in JCPDS card (No. 36-1451) and there was no characteristic peaks of impurities observed. The sharpness of the diffraction peaks suggests that the ZnO sample should be well crystallized.

3.2. The morphology of the ZnO sheets

SEM and TEM images of the pure ZnO sheets are presented in Fig. 3. From Fig. 3(a), it can be seen that the ZnO sheets are very thin with no uniform structure. Fig. 3(b) exhibits the shape as sheet of ZnO nanoparticles. High-resolution TEM (HRTEM) image of an individual ZnO sheet shown in Fig. 3(c) reveals that the interplanar spacing is 0.26 nm, which corresponds to the (0 0 0 1) crystal plane of ZnO crystal. The high-resolution image indicates that the ZnO sheets are single crystal and grow along the (0 0 0 1) direction. In Fig. 3(c), we can see that the lattice lines of ZnO is very obscure, this is because of unstabilized crystal of ZnO under the higher energy electrons. Fig. 4 shows the typical SEM and TEM images of the Ag-stabilized ZnO nanosheets. Representative low-magnification SEM image of the Ag-stabilized ZnO nanocomposites is illustrated in Fig. 4(a), where the ZnO sheets are not obvious on the surface in comparison with Fig. 3(a). The TEM image of the Ag-stabilized ZnO

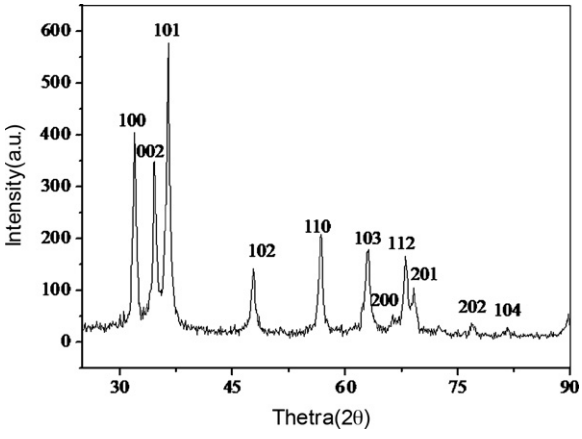

Fig. 2. XRD patterns of pure ZnO nanosheets dried at the temperature of 130 °C.

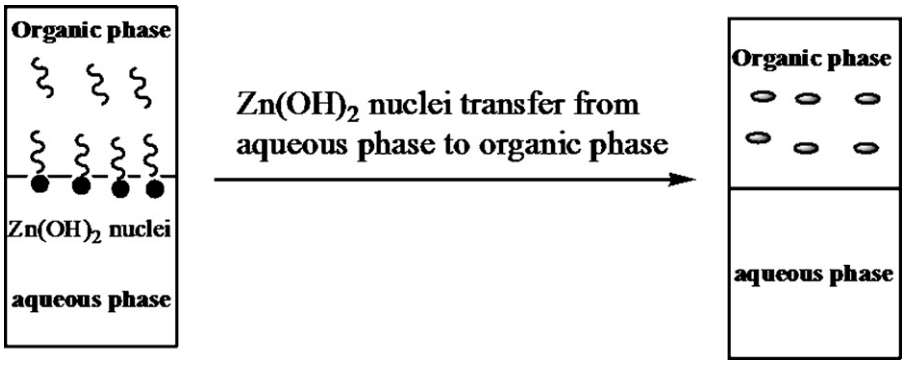

Scheme 1. The formation process of ZnO sheets.

nanocomposites is shown in Fig. 4(b). It can be clearly observed that the silver nanoparticles loaded on the surface of ZnO sheets. The size of Ag nanoparticles ranges from 5 nm to 15 nm. The measured average diameter of the Ag nanoparticles is about 10 nm. The HRTEM image in Fig. 4(c) reveals the lattice spacing of $d = 0.236$ nm, corresponding to the (1 1 1) planes of the metallic Ag with fcc structure. The result demonstrates that the Ag nanoparticles in the nanocomposites are metallic single crystalline Ag with fcc structure, which is in good agreement with the XRD result. Overall, we can make a comparison between Fig. 3(b) and Fig. 4(b) and conclude that the silver nanoparticles can stabilize ZnO nanosheets under the higher energy electrons. Furthermore, the results of the Fig. 3(c) and Fig. 4(c) are well correspond with the XRD which is shown in Fig. 2(b and c).

3.3. UV–vis absorption spectra

The optical absorption spectra of pure Ag nanoparticles, ZnO sheets and Ag nanoparticles stabilized ZnO sheets are shown in Fig. 5. The pure ZnO sheets exhibit UV absorption at 362 nm, as shown in Fig. 5(b). This peak is the exciton absorption of ZnO sheets. The pure Ag nanoparticles samples were prepared through the reaction of Ag^+ and sodium borohydride solution using the same method without adding of zinc acetate dihydrate. The amount of Ag^+ and sodium borohydride solution is the same as the synthesis of Ag nanoparticles in the presence of zinc acetate dihydrate. The pure Ag nanoparticles are in the range of 5–10 nm, with an average size of 8 nm, a little smaller than the Ag nanoparticles coated on the ZnO sheets (Fig. 4(c)). The surface plasmon absorption of Ag nanoparticles prepared by two-phase method in the absence of zinc acetate dihydrate is very narrow and centered at 420 nm (Fig. 5(a)). However, the absorption of the Ag nanoparticles stabilized ZnO sheets is not a simple super-position of those of their individual single-component materials. As can be seen from Fig. 5(c), the surface plasmon band of Ag nanoparticles stabilized ZnO sheets nanocomposites shows a red shift of 27 nm compared to pure Ag nanocrystals. The quantum size effect can be ruled out because the Ag nanoparticles coated on the ZnO sheets are larger than those pure Ag nanoparticles.

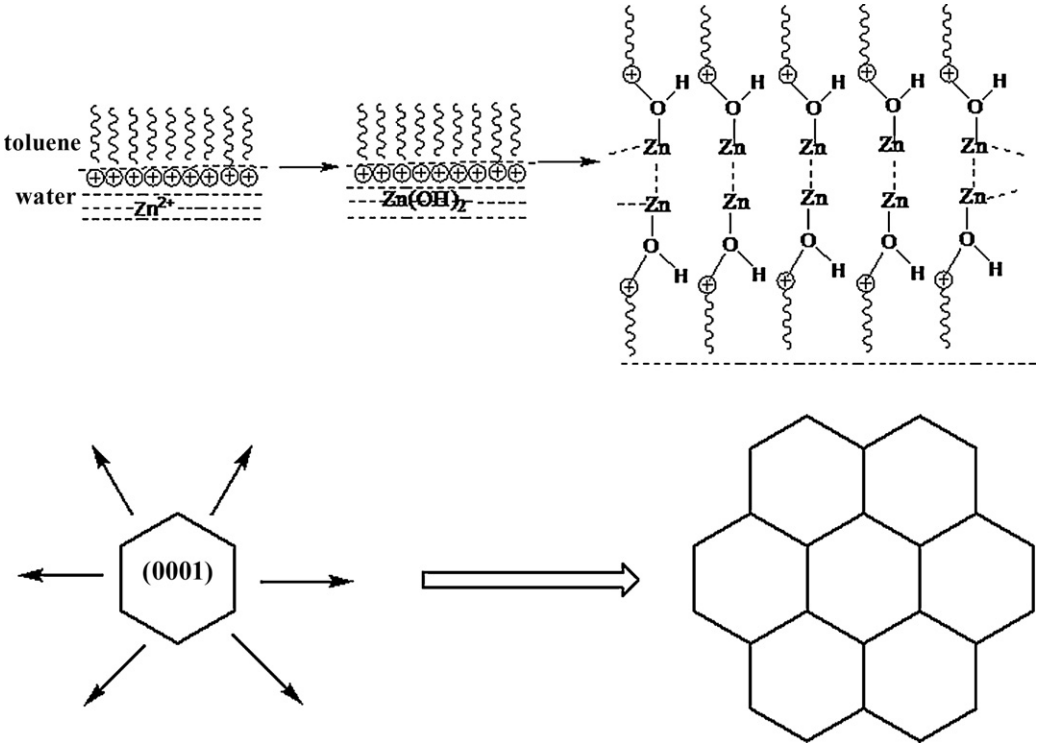

Scheme 2. The formation mechanism of ZnO sheets.

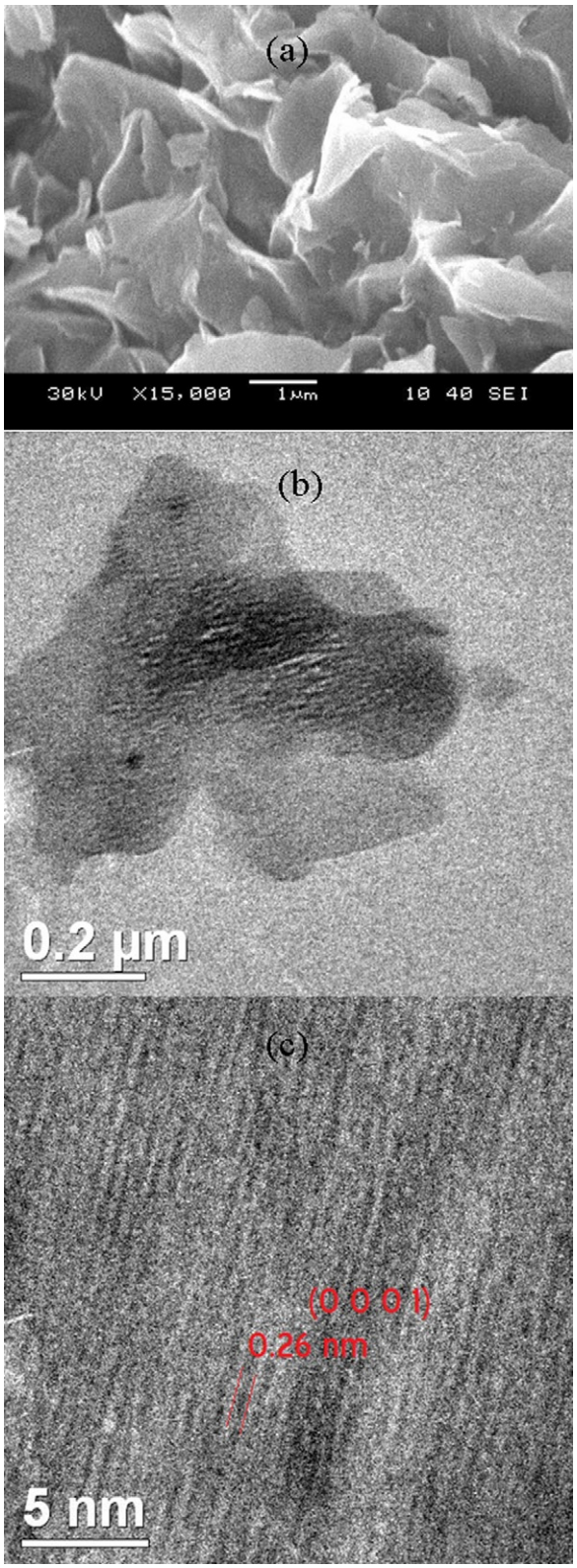

Fig. 3. The SEM and TEM images of ZnO sheets (a) low-magnification SEM image, (b) TEM image and (c) high-resolution TEM image.

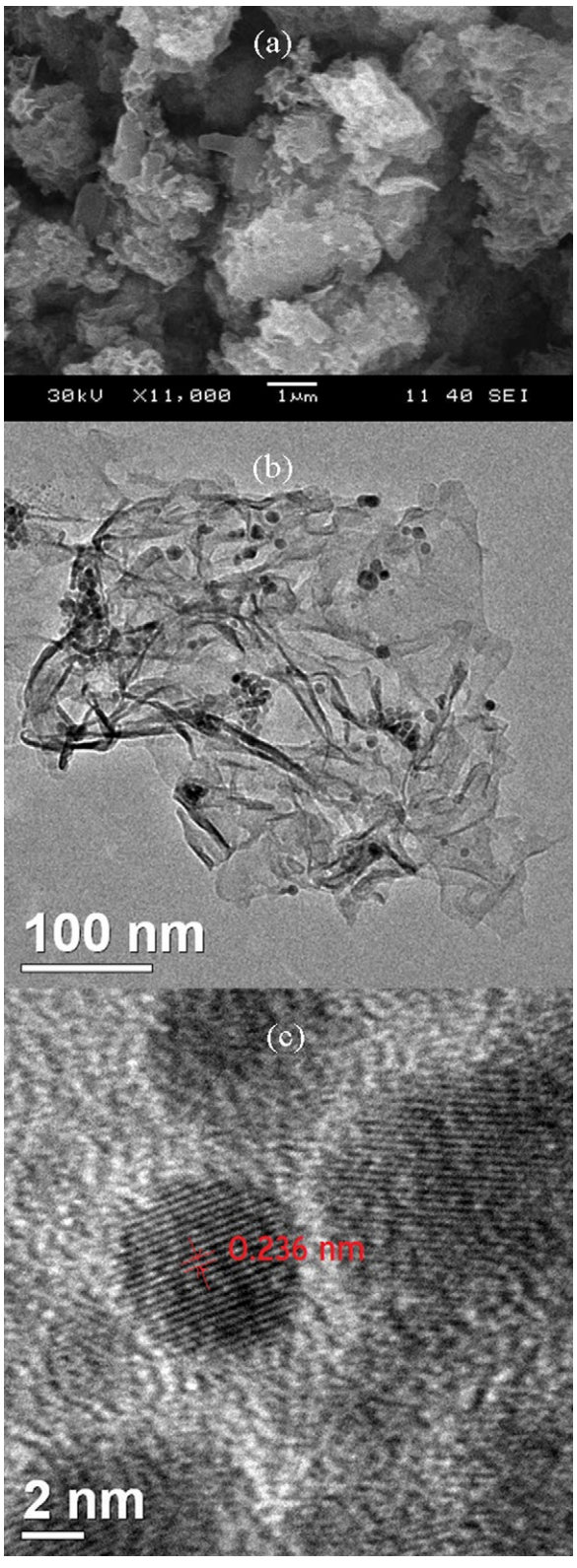

Fig. 4. The SEM and TEM images of Ag nanoparticles stabilized ZnO sheets (a) low-magnification SEM image, (b) TEM image and (c) high-resolution TEM image.

The reason for the red shift of the surface plasmon absorption is due to the strong interfacial coupling between neighboring nanoparticles. In detail, electron transfers from Ag to ZnO in ZnO sheets stabilized by Ag nanoparticles because the Fermi energy level of Ag is higher than that of ZnO, resulting in the deficient electrons on the surface of the Ag nanoparticles. Therefore, the deficient electrons on the surface of the Ag nanoparticles subsequently lead to the red shift of the surface plasmon absorption. Then the surface plasmon band of Ag nanoparticles red shifted nearly 27 nm and the size of silver nanoparticles became larger. The UV absorption

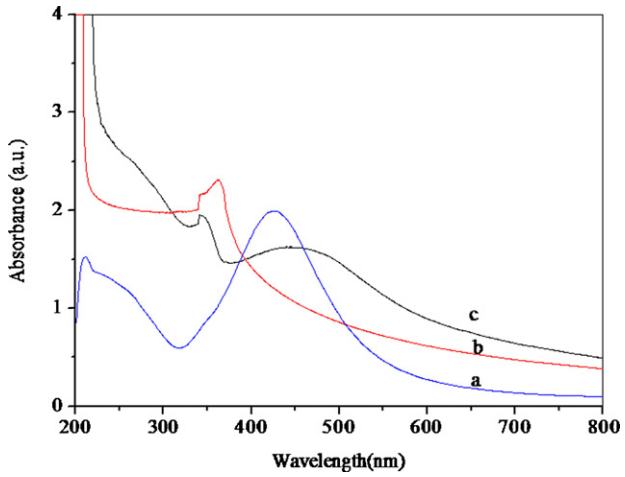

Fig. 5. UV–vis absorption spectra of (a) Ag nanoparticles, (b) pure ZnO sheets and (c) Ag nanoparticles stabilized ZnO sheets.

of Ag nanoparticles stabilized ZnO sheets blue shift by about 5 nm compared to pure ZnO sheets which implies that the size of ZnO sheets (Fig. 4(b)) turn smaller during the synthesis of Ag nanoparticles stabilized ZnO sheets because the absorption shift of pure ZnO nanocrystals is usually related to their sizes' change [19].

3.4. Fluorescence spectra

The photoluminescence spectrum of pure ZnO sheets is shown in Fig. 6(a) and exhibits a shoulder peak centered at about 400 nm and 500 nm, respectively. The two emission peaks can be assigned to the recombination of a photogenerated hole with the single ionized charged state of the defect [20,21]. The growth of Ag nanocrystals onto the ZnO sheets completely quenches the PL, as shown in Fig. 6(b). As we know, the emission peaks at 400 nm and 500 nm is due to the defect-related emissions. On one hand, the defect-related emission peaks can be reduced by the surface modification on ZnO sheets, on the other hand, silver nanoparticles can promote the separation of photo-induced electrons and holes [14].

3.5. The formation mechanism of ZnO sheets stabilized by silver nanoparticles

The ZnO sheets were synthesized by using the liquid–liquid two phase reaction conditions and the formation mechanism was shown below:

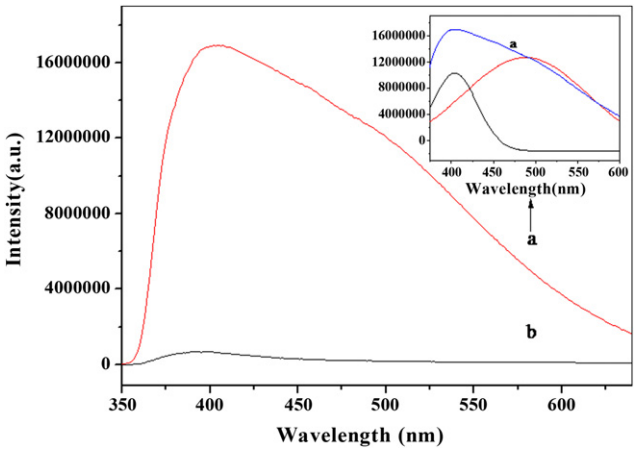

Fig. 6. Fluorescence spectra of (a) pure ZnO sheets and (b) Ag-stabilized ZnO sheets.

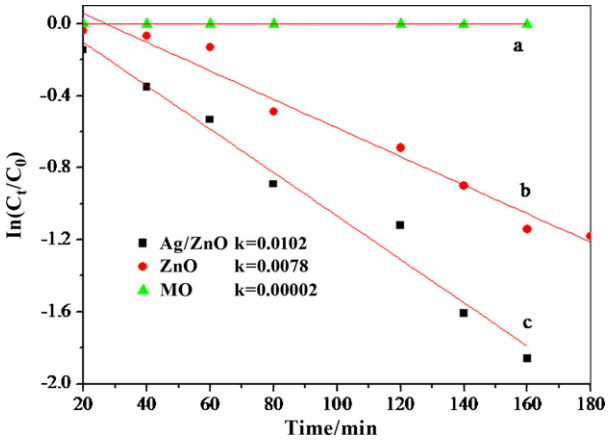

Fig. 7. MO degradation curves of ln(Ct/C0) versus time (t) for photodegradation with different catalysts (a) no catalyst (b) pure ZnO and (c) Ag–ZnO nanosheets; and the reaction rate constant k, from linear fitting.

Firstly, $Zn(CH_3COO)_2$ is in the water phase, where the hydrolyzation reaction is occurred completely.

$$Zn(CH_3COO)_2 + 2H_2O \rightarrow Zn(OH)_2 + 2CH_3COOH \quad (1)$$

Due to a large number of DTAB (cationic surfactant), which can form lamellar micelle, $Zn(OH)_2$ can interact with it thoroughly and the result is that $Zn(OH)_2$ is surrounded by the surfactant which can make them transfer into organic solvents, where the ZnO is formed finally (Scheme 2).

As we know, ZnO belongs to hexagonal system, the cell parameter: $a = 0.3249$ nm, $c = 0.5206$ nm. On the basis of discussion mentioned above and the result of TEM, it can be concluded that the growth of crystal orients along the (0 0 0 1) facet to form various structures which consisted of units of hexagons.

3.6. Photocatalytic testing

The photocatalytic activities of the pure ZnO and Ag/ZnO nanosheets were evaluated by the degradation of methyl orange (MO) dye under UV irradiation. The degradation is monitored by studying the decrease in absorbance of methyl orange in presence of powder sample suspensions and quantified by plotting a first order decay plot of the absorbance at 463 nm. The first-order rate constant for degradation, k, can be obtained from the first-order plot according to the following Eq. (1) [22]:

$$\ln\left(\frac{C_t}{C_0}\right) = -kt \quad (2)$$

where C_0 is the initial concentration and C_t is the concentration after the MO degradation for time t. Fig. 7 shows the photodegradation curves of MO in the form of $\ln(C_t/C_0)$ as a function of time and the determined values of the reaction rate constant, k, from linear fitting for different samples.

In Fig. 7, the blank test shows that the degradation of methyl orange changes little after irradiation, indicating that the photo induced self-decomposition can be neglected in comparison with the photo catalysis caused by catalyst particles [15]. Thus, the UV-light-induced degradation of methyl orange in our work can be evaluated as a real photo catalytic activity of the pure ZnO and Ag-stabilized ZnO sheets, respectively. Notably, in Fig. 7, the Ag/ZnO nanosheets exhibit higher photocatalytic activity compared to the pure ZnO nanosheets. The improved photocatalytic activity of Ag/ZnO composite is probably due to the more effective electron–hole separation of the Ag/ZnO composite. Some similar report [23] indicates Ag nanoparticles, acting as electron sinks, can reduce the recombination of photoinduced electrons and holes and

prolong the lifetime of the electron pairs. Hence, based on their excellent photocatalytic performance, the Ag/ZnO nanosheets are possibly favorable for potential application in purification of polluted water or air.

As the photocatalytic process of the Ag/ZnO composite is complex and controversial, here we would like to discuss it in detail by proposing the band structure of the Ag/ZnO. As we know, the work function of ZnO (5.2 eV) is larger than that of Ag (4.26 eV), implying that the electrons will migrate from silver to the conduction band (CB) of ZnO to achieve the Fermi level equilibration when they get into contact. The process can be expressed as:

$$Ag \rightarrow Ag^{+} + e^{-} \quad (3)$$

When the catalysts are illuminated by UV light with photon energy higher than the band gap of ZnO, electrons (e^{-}) in the valence band (VB) can be excited to the CB with simultaneous generation of the same amount of holes (h^{+}) left behind.

The photocatalytic reaction can be thus expressed as follows [24]:

$$ZnO + h\nu \rightarrow h^{+} + e^{-} \quad (4)$$

$$h^{+} + OH^{-} \rightarrow {}^{\bullet}OH \quad (5)$$

$$h^{+} + H_2O \rightarrow {}^{\bullet}OH + H^{+} \quad (6)$$

$$e^{-} + Ag^{+} \rightarrow Ag \quad (7)$$

$$e^{-} + O_2 \rightarrow {}^{\bullet}O_2^{-} \quad (8)$$

$${}^{\bullet}O_2^{-} + H^{+} \rightarrow {}^{\bullet}O_2H \quad (9)$$

$$2{}^{\bullet}O_2H \rightarrow H_2O_2 + O_2 \quad (10)$$

4. Conclusions

In summary, we have developed a facile and general strategy for the synthesis of ZnO sheets. Detailed structural characterization and elemental analysis demonstrate the presence of ZnO sheets, loaded by Ag nanoparticles. The synthesis employs ZnO sheets as the substrates, where silver seeds are grown on the surface, and make the ZnO sheets more stabilization. The photocatalysis test shows that the ZnO sheets stabilized by silver nanoparticles exhibit a higher photocatalytic activity than the pure ZnO nanosheets, thereby implying that the Ag/ZnO interfaces promote the separation of photogenerated electron–hole pairs and enhance the photocatalytic activity.

Acknowledgements

This work was financially supported by the National Natural Science Foundation of China (No. 10776014) and also by the High Technical Foundation of Jiangsu Province of China (No. BG2007047).

References

[1] J. Lu, K.M. Ng, Ind. Eng. Chem. Res. 47 (2008) 1095–1101.
[2] J.H. Lim, C.K. Kong, K.K. Kim, I.K. Park, D.K. Hwang, S.J. Park, Adv. Mater. 18 (2006) 2720–2724.
[3] M.T. Mohammad, A.A. Hashim, M.H. Al-Maamory, Mater. Chem. Phys. 99 (2006) 382–387.
[4] J.H. Kim, Y.C. Hong, H.S. Uhm, Surf. Coat. Technol. 201 (2007) 5114.
[5] M.S. Tokumoto, V. Briois, C.V. Santilli, J. Sol. Gel. Sci. Technol. 26 (2003) 547–551.
[6] J. Zhang, L.D. Sun, J.L. Yin, H.L. Su, C.S. Liao, C.H. Yan, Chem. Mater. 14 (2002) 4172–4177.
[7] M.M. Demir, R. Munoz-Espi, I. Lieberwirth, G. Wegner, J. Mater. Chem. 16 (2006) 2940–2947.
[8] S. Park, K.R. Lee, C.H. Jung, S.J. Kim, H.C. Shin, Jpn. J. Appl. Phys. 35 (1996) L996.
[9] X. Zhao, B. Zheng, C. Li, Powder Technol. 100 (1998) 20–23.
[10] J.Y. Li, X.L. Chen, H. Li, J. Cryst. Growth 233 (2001) 5–7.
[11] Z.R. Dai, Z.W. Pan, Z.L. Wang, Adv. Funct. Mater. 13 (2003) 9–24.
[12] R. Radoi, P. Fernandez, J. Piqueras, M.S. Wiggins, J. Solis, Nanotechnology 14 (2003) 794–798.
[13] L. Shen, N. Bao, K. Yanagisawa, K. Domen, A. Gupta, C.A. Grimes, Nanotechnology 17 (2006) 5117–5123.
[14] R. Georgekutty, M.K. Seery, S.C. Pillai, J. Phys. Chem. C 112 (2008) 13563–13570.
[15] Y.G. Chang, J. Xu, Y.Y. Zhang, S.Y. Ma, L.H. Xin, L.N. Zhu, C.T. Xu, J. Phys. Chem. C 113 (2009) 18761–18767.
[16] H. Zeng, W. Cai, P. Liu, X. Xu, H. Zhou, C. Klingshirn, H. Kalt, ACS Nano 2 (2008) 1661–1670.
[17] L.H. Li, J.C. Deng, H.R. Deng, Z.L. Liu, X.L. Li, Chem. Eng. J. 160 (2010) 378–382.
[18] F. Li, J.F. Wu, Q.H. Qin, Z. Li, X.T. Huang, Superlattices Microstruct. 47 (2010) 232–240.
[19] T. Yatsui, S. Sangu, T. Kawazoe, M. Ohtsu, S.J. An, J. Yoo, G.C. Yi, Appl. Phys. Lett. 90 (2007) 223110–223112.
[20] K. Nomura, H. Ohta, K. Ueda, T. Kamiya, M. Hirano, H. Hosono, Science 300 (2003) 1269–1272.
[21] N. Yamazoe, Sens. Actuators B 5 (1991) 7–19.
[22] C.D. Gu, C. Cheng, H.Y. Huang, T.L. Wong, N. Wang, T.Y. Zhang, Cryst. Growth Des. 9 (2009) 3278–3285.
[23] J.S. Xie, Q.S. Wu, Mater. Lett. 64 (2010) 389–392.
[24] D.D. Lin, H. Wu, R. Zhang, W. Pan, Chem. Mater. 21 (2009) 3479–3484.